NUMERICAL ANALYSIS OF MECHANICAL PROPERTIES OF AUXETIC CELLULAR MATERIAL CONSISTING OF RE-ENTRANT HEXAGONAL, HONEYCOMBS AND STAR-FISH

Khalissa SAADA [1,2,*],Salah AMROUNE[1,2] ,Moussa ZAOUI[1,2],Amin HOUARI[3],Chouki FARSI[1,2], Fares Mohammed Laid REKBI[4],Kouider MADANI[3]

[1]*Department of Mechanical Engineering, University of Mohamed Boudiaf-M'Sila, Algeria.*
[2]*Laboratoire de Matériaux, et Mécanique des Structures (LMMS), Université de M'sila. Algérie.*
[3]*Laboratoire de Matériaux, et Mécanique des Structures (LMMS), Université SBA. Sidi Bel Abesse, Algérie.*
[4]*Research Center in Industrial Technologies (CRTI), P.O. Box 64, Cheraga 16014, Algiers, Algeria*
E-mail: khalissa.saada@univ-msila.dz

AJME 2025, 23 (1).https://doi.org/10.5281/zenodo.15044094

ABSTRACT: *Sandwich panels are important because they offer a lightweight and economical structure that can be used in various fields and has several geometric shapes. For this study, we chose three honeycomb shapes (Hexagonal, RE-entrant and Star fish) with dimensions of 57mm×120mm and a thickness of 10mm. Aluminum type (Al 2024-T3) was used for the material. The design of the three honeycomb structures was carried out with CATIA V5R20 software, while the numerical analysis of their load capacity (tensile and compression) was carried out using the ABAQUS-CAE calculation code. A numerical study was also carried out to compare the results of the samples according to the different types of honeycomb used. The results showed that the RE-shaped structure had the highest load capacity in terms of tensile and compression. The maximum stress of 422.27 MPa was observed for the honeycomb-shaped structure RE-entering in traction. In contrast, the maximum tensile stress was lower for the starfish-shaped honeycomb, reaching a value of 145.5 MPa. For compression, the hexagonal honeycomb structure recorded the highest stress value of 590.5 MPa. The lowest stress value was measured for the starfish-shaped honeycomb structure, reaching 199.5 MPa.*

KEYWORDS: *Honeycomb,RE-entrant,Star-Fish,load-displacement, Finite element analysis*

1 INTRODUCTION

In recent years, shipbuilding and aerospace have used honeycomb structures made from different materials for sandwich panels. In particular, hexagonal honeycombs are preferred because of their lightness and reduced cost.[1]. These structures are also used in other fields such as automotive, aviation and transport.[2-4]. Honeycomb structures come in different shapes, including the hexagonal shape [5-8]

There are also other shapes such as circular shaped structures [9] , Re-entrant [10-12], hexagonal and RE- entrant [13-15], triangular and other model [16] and star-Fish [17].

Several studies have focused on characterizing honeycomb structures both numerically and experimentally to achieve mechanical properties such as traction, compression and torsion. For example, Krishna et al. [2] Used the hexagonal titanium and aluminum honeycomb structure for bending tests on an ANSYS calculation code. The authors concluded that the titanium structure is better than the aluminum one, but it is expensive and heavier. Tabacu and Ducu. [18] erformed a compression test on a set of structures, including a hive structure, a lattice structure, a honeycomb structure and a rectangular structure. Both researchers noted that there was convergence between experimental and numerical results. Ghongade et al. [19] studied honeycombs with a circular structure (with and without reinforcement) in which a set of steel tubes were welded. A numerical analysis of the compression loads was performed using ABAQUS software and it was found that the reinforced honeycombs had the highest bearing capacity. Xia et al. [20] studied three aluminum alloy structures inspired by a honeycomb. The authors applied axial compression to the samples to measure energy absorption, in the same way. Xu et al. [21] made honeycomb (re-entrant) samples filled with aluminum foam and noticed that aluminum foam increased energy absorption resistance due to its compressive strength. Ganesh et al. [22] performed bending tests on hexagonal honeycomb structures made of aluminum, titanium and steel using CATIA and ANSYS software. They noted that aluminum and titanium have higher bending strength than steel, but titanium is also heavier.

In this article, we digitally studied three different types of aluminum honeycombs (Hexagonal, Re-entrant and Star- fish) (Al 2024-T3). The samples were designed in the CATIA program. In addition, the ABAQUS program was used to know and improve their mechanical properties. We applied traction and compression to the samples. Finally, we compared the results of samples from different structures to understand the geometric effect of honeycombs on their mechanical properties. The objective of this study was to select the best structure among the three geometric shapes proposed in terms of mechanical properties for later use in bio-composite structures (Epoxy/palm fibers).

2 THEORETICAL FRAMEWORK

The honeycombs studied in this article are subjected to an F-force, which can be a tensile or compressive force. The stress force along the S section can be calculated using the following equation: [23, 24]

$$F_s = \int_{dS} \sigma dS \quad (0)$$

$$F_e = \sigma_e * S_e \quad \text{(Inelastic level)} \quad (2)$$

$$F_e = E_e * \varepsilon_e * S_e \quad \text{(Elastic Level)} \quad (3)$$

$$\sigma = \frac{f_s}{1.5}\left(1-\left(1-\frac{\varepsilon}{0.02}\right)^2\right) * 0.85 \quad (4)$$

Then, the quasi-static stress of the tray σ the auxetic honeycomb was given by [25]:

$$\sigma = \frac{\int_0^N \sigma(\varepsilon) d\varepsilon}{N} \quad (5)$$

Where σ (ε) and ε are compressive strain, crushing stress respectively and N is densification strain.

The Jones-Wilkens-lee equation is used to calculate the pressure generated as shown in the equation (6)[26]:

$$P = b_1\left(1-\frac{\eta}{C_1 V}\right)e^{-CV} + b_2\left(1-\frac{\eta}{C_2 V}\right)e^{-CV} + \left(\frac{\eta E}{V}\right) \quad (6)$$

Where V is the relative volume of the explosive product, E is the internal energy per unit volume, b_1 , b_2, C_1 , C_2 , η, are empirically constant derivatives for explosives (Abaqus/CAE).

Method was used to measure voltage. To calculate the Poisson coefficient of the sample and can be calculated the longitudinal elongation. Can calculate by the following formula [15]:

$$\nu_{jk} = -\frac{\varepsilon^y_{jk}}{\varepsilon^z_{jk}} = -\frac{\Delta^y_{jk}}{\Delta^z_{jk}} \cdot \frac{A_z}{A_y} = -\frac{\left[Y_{j(k+1)} - Y_{j(k-1)}\right]}{\left[Z_{k(j+1)} - Z_{k(j-1)}\right]} \cdot \frac{A_z}{A_y}$$

$$(2 \le j \le 3, 2 \le k \le 3) \quad (7)$$

$$\overline{\nu} = \frac{1}{4}\sum \nu_{jk} \quad (8)$$

where: ν_{jk} is the Poisson coefficient, AZ, Dy are respectively the horizontal and vertical distances of consecutive points of undeformed specimens, ε^y_{jk} transverse deformation ε^z_{jk} ε^y_{jk} axial deformation, Y. Z are the real-time coordinates of the points.

The Hu-Washizu form of the mechanical problem is defined by the minimization problem of functional. The Solid deforms under the effect of density forces f_V, it is subject to forces imposed t_N on ∂NS0 [27].

$$k(u, \mathrm{H}, \mathrm{P}) = \int_{S_0} \psi_{mec}(F) + (\nabla_x u - H) : \int_{S_0} f_V . u - \int_{\partial_N S_0} t_N . u \quad (9)$$

Where: u is displacements , is the gradient of the displacement field , P the first PiolaKirchoff tensor , ψ_{mec} denotes the mechanical energy potential of the system and the gradient of the transformation.

3 GEOMETRY OF MICROSTRUCTURES AND REPRESENTATIVE VOLUME ELEMENT

There are many types of artificial honeycombs. In this study, we chose to work with three types of honeycomb structures (Hexagonal, Re-entrant and Star -fish), which have also been used in other research (as indicated in the references [13, 28, 29]. As shown in Fig.1, the Star fish structure has 30 cells with a size of 121mm × 57mm × 10mm, resulting from a number of cells of 3 × 4 (width × height). The honeycomb structures were designed using CATIA software, with dimensions of 127×20×10mm3 for each cell unit manufactured with dimensions of 18×21×10mm3. The different dimensions of the honeycombs used are presented in the table. The designed honeycombs were then digitally analyzed using ABAQUS software.

Table 1. Dimensions of the different honeycombs studied

	Length(mm)	Width(mm)	Pate thickness (mm)	Thickness (mm)	Cell length (mm)	Cell side length (mm)
Honeycombs	H	W	ep	e	Lc	Lcs
Hexagonal	121.8	57	10	3	15	8.66
Re - entrant	114.6	57	10	3	15	9.199
Star- fish	127	58.2	10	3	17.176	13.65

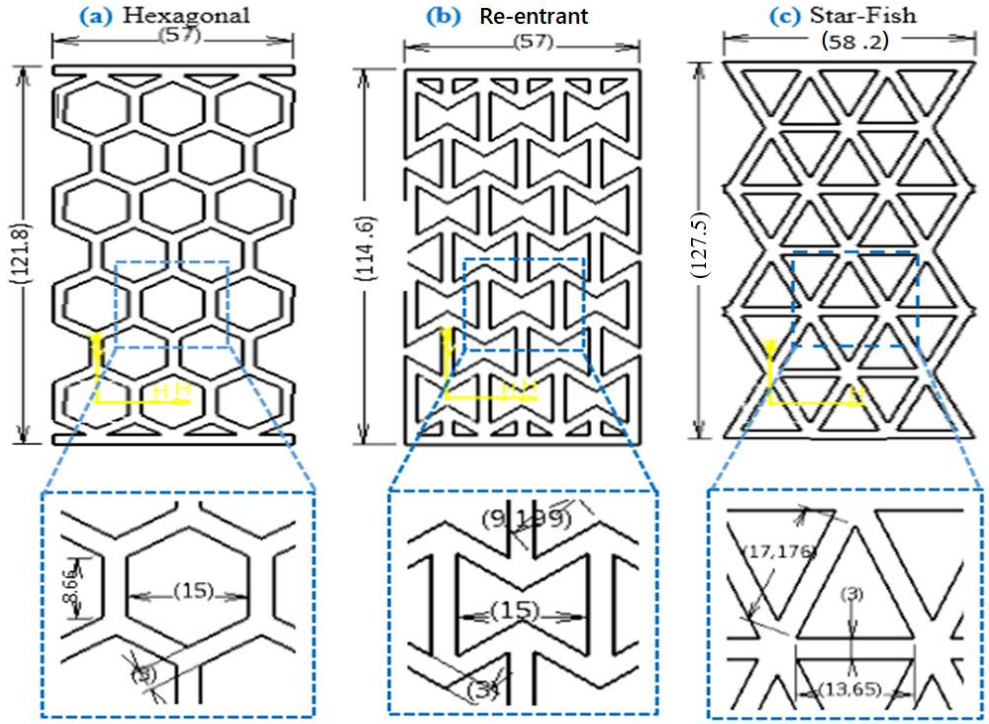

Fig.1 Microstructure textures at different scales: a) hexagonal, b) RE- entrant c) star-fish

4 MATERIALS AND METHODS

The honeycomb structure was made of Al 2024-T3 aluminum with a thickness of 3mm. The mechanical properties are presented in Table 2. Aluminum alloy 2024-T3 has a set of mechanical properties that make it an excellent material. With a density of 2.52g.cm-3 it is light and therefore very interesting, especially for applications in the aerospace sector. Many researchers have also studied the interface.[21, 30].

Table 2. Mechanical properties of Aluminum alloy 2024-T3

Material	σ_{R}(MPa)	$\sigma_{0.2}$(MPa)	E(MPa)	A(%)	v
Al 2024-T3	452	230	73800	2.4	0.33

5 NUMERICAL ANALYSIS

5.1 Finite element modeling (FE)

This analysis was performed digitally using the general purpose finite element software ABAQUS v16.14. The mesh layout was used for each type of honeycomb (Hexagonal, Re-entrant and Star- fish) using 3D Continuum hexahedral elements (type ABAQUS C3D8R) for all volumes from 57 × 120 × 10mm3, indicating the autonomy of the models. Finally, a mesh grid of overall size of about 1mm was chosen for the division of each element, giving this division 29,840 nodes and 37,570 elements. The results of this analysis are presented in Table 3.

Table 3. The input parameter is the mesh part

Type of honeycomb	Type of mesh	Approximate global size	Number of nodes	Nombre of elements.
Hexagonal	Continuum-3D hexagonal C3D8R	1	29 840	37 570
RE-entrant	Continuum-3D hexagonal C3D8R	1	29 840	37 570
Star fish	Continuum-3D hexagonal C3D8R	1	29 840	37 570

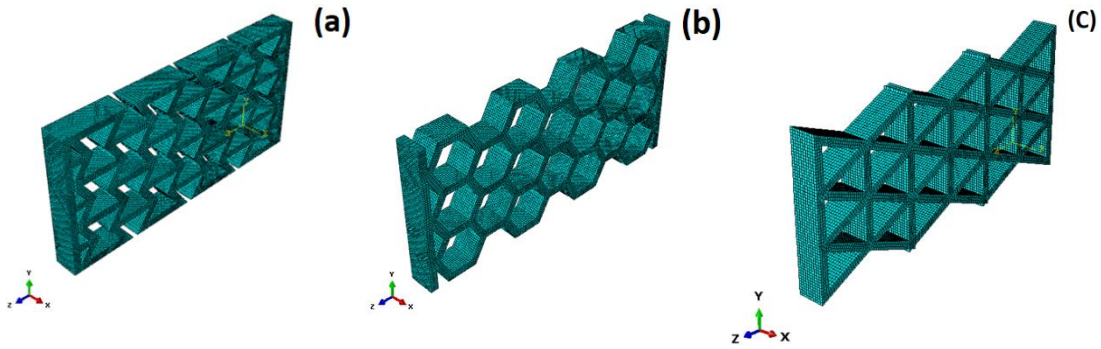

Fig.2 Three models of honeycombs (3D) in structured mesh form (a) RE-entrant (b) hexagonal (c) star-fish.

6 NUMERICAL RESULTS AN DISCUSSION

6.1 Traction

6.1.1 Stress analysis

In the case of tensile in the direction (z) shown in Fig. 3.stress localization occurs in different regions, and stress is concentrated in the angle of inclination at the cell walls for RE-entrant, hexagonal and star-Fish models. The tensile test also shows that the maximum stress of a hexagonal cell is 485.6 MPa, while for the RE-entrant and star-Fish models, the stress values are 367.4 MPa and 212.6 MPa, respectively. In addition, the stress of the star-Fish at the top is greater than that of the lower star-Fish.

The same strain patterns were observed for all models, as shown in Fig. 4. The hexagonal of the dam undergoes a displacement of 1.056 mm in case of traction, which is higher than the displacement of RE-entrant and star-Fish, which are respectively 0.08335 mm and 0.2311 mm. The maximum displacement is detected at the hexagonal level.

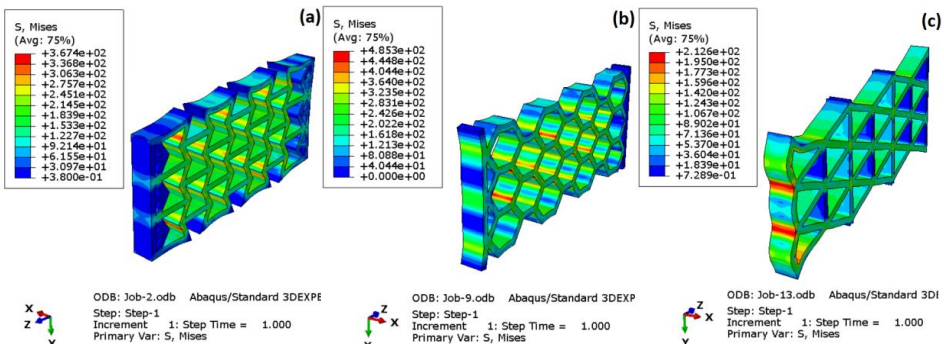

Fig.3 Distribution of stresses after traction: a) RE-entrant,b) hexagonal and c) star-fish.

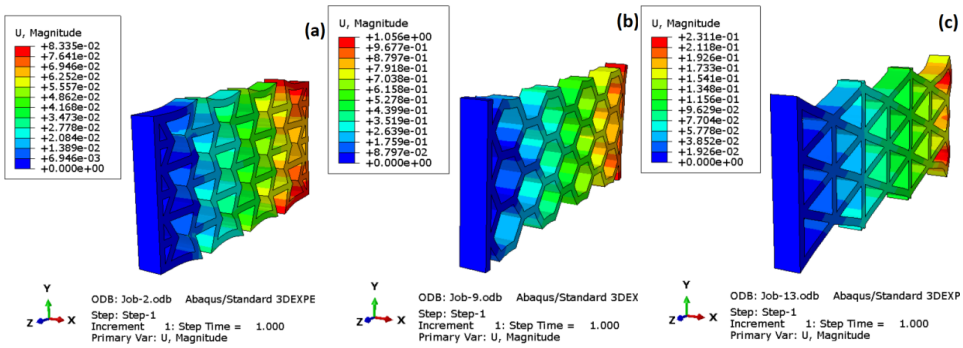

Fig.4 The displacement values [mm] for the three models with the applied voltage pressure of 50MPa: a) RE-incoming, b) hexagonal and c) star-Fish.

In this study, we compared numerical predictions of honeycomb sandwiches and force-displacement relationships with experimental data, as shown in Fig. 5. The behavior can be divided into two distinct stages: an initial linear step in which the curves rise steadily and linearly, indicating that the specimens are in the elastic domain, followed by a tray step in which the stiffness of the honeycomb sandwiches gradually decreases, and the specimens pass into the plastic domain. We recorded a maximum force of about 105 N for a 5 mm displacement of the RE-entrant honeycomb sandwich, and a minimum force of about 4 × 104 N for a 3.4 mm displacement of the hexagonal honeycomb sandwich. On the other hand, there is a clear improvement in results for the honeycomb sandwich with a RE-entrant structure, which is due to the difference in structure of honeycomb sandwiches for the three models presented in this article.

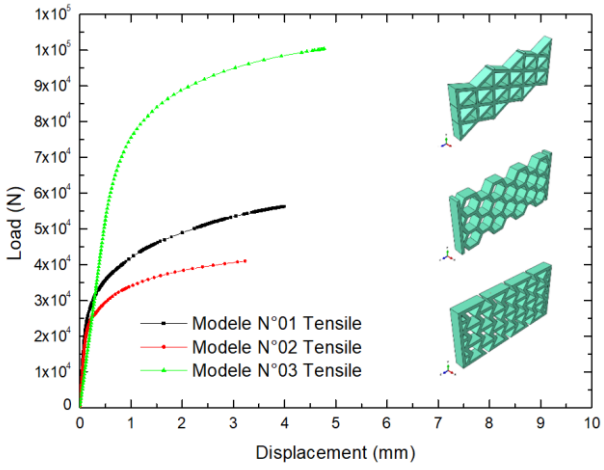

Fig.5 The force-displacement curves of the tensile test for the three models studied.

Table 4 presents the results of the numerical tensile comparison for each of the stresses, displacements and strains of the three axes xx, yy and zz. It is observed that the deformation rate was high for the hexagonal honeycomb, while it was lower for a honeycomb with a RE-entrant structure. The stress value was high in the hexagonal honeycomb, while it was lower in the Star-Fish honeycomb. As for the movement on the three axes for each of the three types of honeycombs, they were different.

Table 4. Comparison between numerical results for the three specimens on ABAQUS for traction

		Hexagonal	**RE-entrant**	**Star fish**
Magnitude (MAX) (mm)	U11	7.965E-3	6.515E-4	4.609E-3
	U22	2.253E-1	2.285E-2	4.359E-2
	U33	4.875E-3	1.321E-3	2.377E-4
STRESS (MAX) (MPa)	S11	1.41E2	1.448E2	6.680E 1
	S22	3.566E2	4.227E2	1.455E2
	S33	3.377E2	2.651E2	2.086E2
Strain (MAX) (%)	E11	2.058E-3	1.389E-4	8.094E-4
	E22	3.927E-3	4.543E-4	1.860E-3
	E33	3.711E-3	3.321E-4	2.376E-3

6.2 Compression

6.2.1 Stress analysis

Due to its high tensile strength, the stress behaviour of the three models is identified in the graph in Fig. 6. when subjected to loads. Then, the stress results are compared for the three models (RE-entrant, hexagonal and star-Fish) using numerical resolution during compression loading. The numerical results demonstrated that the geometries of the three hexagonal mechanical models cause stiffening of the structure in the impact region.

Further studies are needed to fully study and understand this complex and challenging topic, and to develop more elaborate models in order to obtain more realistic constraints. The numerical simulation results (force-displacement and damage mapping) performed with ABAQUS are shown in Fig.6.for the RE-entrant, hexagonal and star-Fish models.

The section of the structures directly influences their performance. The best stress was obtained for hexagonal structures (NH) with a value of 488.4 MPa, which represents an increase of 24.77% compared to the lowest stress value for the re-entrant model (RE-NH) (367.4 MPa). On the other hand, the lowest impact resistance performance was obtained for the Star-Fish honeycomb sandwich (S-F). This condition is associated with small deformations as well as the appearance of cracks from the first impacts of buckling phenomena.

cracks from the first impacts of buckling phenomena.

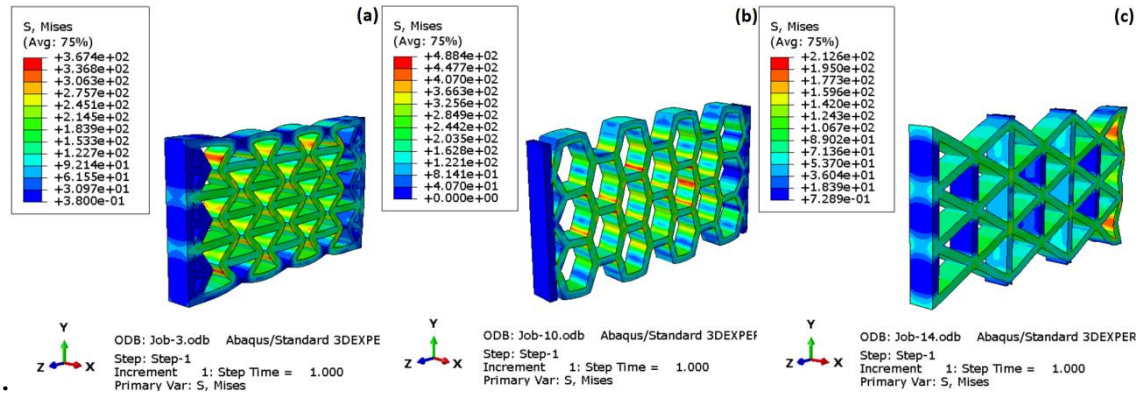

Fig. 6 Stress distribution after compression: a) RE-incoming, b) hexagonal and c) star-fish.

The deformation phenomenon is visible in Fig.7. Which shows the results of the simulation performed with the ABAQUS/CAE software on the model of sandwich structure damaged under compression. Fig.11. shows the deformation resulting from the RE-entrant model (Fig.11-a.), the hexagonal model (Fig.11-b.) and the star-Fish model (Fig.11-b.).

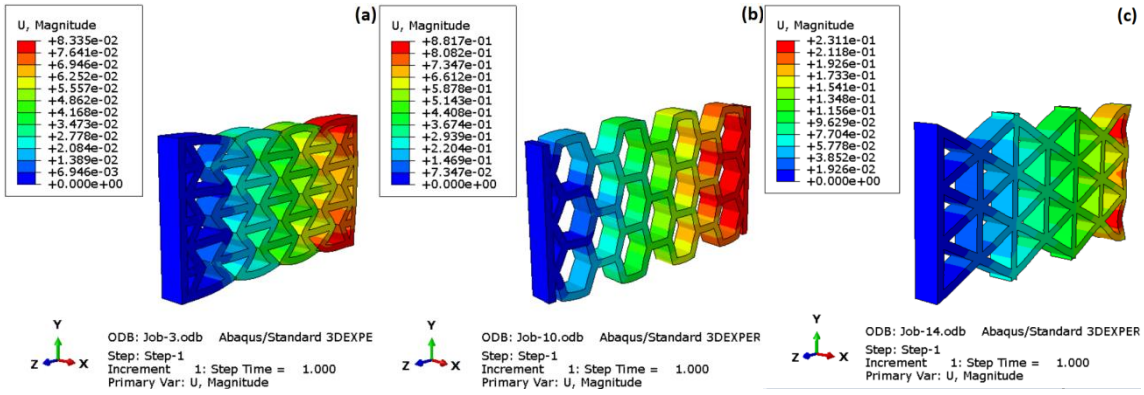

Fig .7 Displacement values [mm] for the three models with the applied voltage pressure of 50MPa: a) RE-entrant, b) hexagonal and c) star-fish

Compression tests were carried out under positional control at a travel speed of 23 mm/min. The results in terms of force-displacement curves for the three honeycomb sandwich models and strain trajectories are shown in Fig.8. The load values are normalized with respect to the number of honeycomb cells in the respective samples. The results show that the compressive force can be quantified as a function of the shape of the honeycomb. For example, in this article, the RE-entrant honeycomb structure records a maximum force of around 105 N for a displacement of 6 mm. In contrast, the other two honeycomb sandwiches hexagonal and star-fish) have almost the same level of strength with similar displacements.

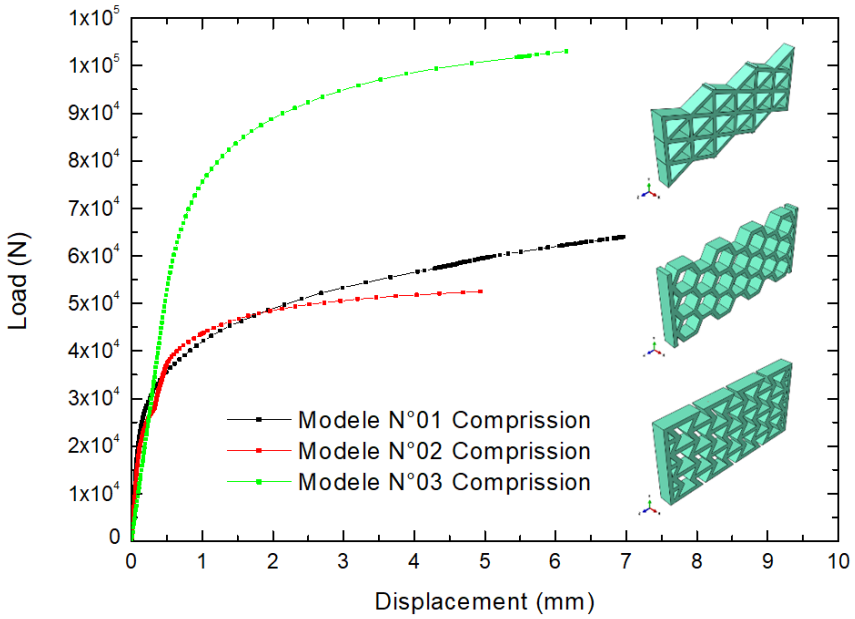

Fig. 8 Represent the force-displacement (Compression) curves for the three models.

Table 5 presents a numerical comparison of stress, strain and displacement during the compression process in the Abaqus program. It is observed that the stress, strain rate and displacement values were high for the three axes xx, yy and zz for the hexagonal honeycomb, while these values were low in the Star-Fish honeycomb.

Table 5. Comparison between numerical results for the three specimens on ABAQUS for compression

		Hexagonal	**RE-entrant**	**Star -fish**
Magnitude (MAX) (mm)	U11	7.965E-3	6.515E-4	4.609E-3
	U22	2.238E-1	2.301E-2	4.343E-2
	U33	8.817E-1	8.012E-2	2.309E-1
STRESS (MAX) (MPa)	S11	2.305E2	8.832E1	5.016E 1
	S22	5.905E2	2.502E2	1.995E2
	S33	1.705E2	1.455E2	4.541E1
Strain (MAX) (%)	E11	2.014E-3	1.412E-4	8.340E-4
	E22	6.634E-3	3.108E-4	2.713E-3
	E33	2.812E-3	2.342E-4	5.940E-4

7 CONCLUSIONS

A detailed analysis and objective comparison of recent studies was conducted on the application of finite element analysis to honeycombs. The Abaqus/CAE software was used to study the effect of traction and compression on different types of honeycombs (RE-entrant, hexagonal and Star-Fish). By comparing the simulation results, we came to the following conclusions:

Loads induce a more localized deformation in the structure, which can lead to an early onset of plasticity and localized instability.

The honeycomb cell with RE-incoming geometry is more suitable to withstand loads such as traction and compression, compared to the

hexagonal honeycomb cell and Star-Fish. The maximum load was reached at 105N for both types of loads.

Finally, the honeycomb structure with RE-entrant geometry has the best impact resistance during axial impacts (tensile and compression). This type of structure can be made of aluminum and used in the equipment of some aircraft, as well as in product packaging. Nevertheless, the use of pure aluminum remains limited due to its poor mechanical properties.

8 REFERENCES

1. Nazeer, S., S. Allabakshu, and P. Student, Design and Analysis of Honey Comb Structures with Different Cases. International Journal of Engineering Development and Research, 2015. 3(4): p. 144-156.

2. Krishna, P.S., A.M. Vemula, P.U. Ahamed, and S. Jani, Bending analysis of honeycomb sandwich panels with metallic face sheets and GFRP core. Materials Today: Proceedings, 2021.

3. Rekbi, F.M.L., M. Hecini, and A. Khechai, Experimental and numerical analysis of mode-I interlaminar fracture of composite pipes. Journal of the Brazilian Society of Mechanical Sciences and Engineering, 2018. 40(10): p. 502. 10.1007/s40430-018-1423-y.

4. Khechai, A., M.-O. Belarbi, A. Bouaziz, and F.M.L. Rekbi, A general analytical solution of stresses around circular holes in functionally graded plates under various in-plane loading conditions. Acta Mechanica, 2022: p. 1-21.

5. Khan, M.S., A. Abdul-Latif, S.S.R. Koloor, M. Petrů, and M.N. Tamin, Representative cell analysis for damage-based failure model of polymer hexagonal honeycomb structure under the out-of-plane loadings. Polymers, 2021. 13(1): p. 52.

6. Audibert, C., A.-S. Andréani, É. Lainé, and J.-C. Grandidier, Discrete modelling of low-velocity impact on Nomex® honeycomb sandwich structures with CFRP skins. Composite Structures, 2019. 207: p. 108-118.

7. Khan, M.S., A. Abdul-Latif, S.S.R. Koloor, M. Petrů, and M.N. Tamin, Representative cell analysis for damage-based failure model of polymer hexagonal honeycomb structure under the out-of-plane loadings. Polymers, 2020. 13(1): p. 52.

8. Li, J., J. Liu, H. Liu, and J. Yang, A precise theoretical model for laterally crushed hexagonal tubes. Thin-Walled Structures, 2020. 152: p. 106750.

9.Tang, H., Q. Wang, G. Yang, J. Gu, N. Liu, L. Jia, and M. Qian, A honeycomb-structured Ti-6Al-4V oil–gas separation rotor additively manufactured by selective electron beam melting for aero-engine applications. JOM, 2016. 68(3): p. 799-805.

10. Indreș, A.I., D.M. Constantinescu, and O.A. Mocian, Bending behavior of 3D printed sandwich beams with different core topologies. Material Design & Processing Communications, 2021. 3(4): p. e252.

11.Shao, Y., J. Meng, G. Ma, S. Ren, L. Fang, X. Cao, L. Liu, H. Li, W. Wu, and D. Xiao, Insight into the negative Poisson's ratio effect of the gradient auxetic reentrant honeycombs. Composite Structures, 2021. 274: p. 114366.

12.Yu, R., W. Luo, H. Yuan, J. Liu, W. He, and Z. Yu, Experimental and numerical research on foam filled re-entrant cellular structure with negative Poisson's ratio. Thin-Walled Structures, 2020. 153: p. 106679.

13. Geramizadeh, H., S. Dariushi, and S.J. Salami, Optimal face sheet thickness of 3D printed polymeric hexagonal and re-entrant honeycomb sandwich beams subjected to three-point bending. Composite Structures, 2022. 291: p. 115618.

14.Namvar, N., A. Zolfagharian, F. Vakili-Tahami, and M. Bodaghi, Reversible energy absorption of elasto-plastic auxetic, hexagonal, and AuxHex structures fabricated by FDM 4D printing. Smart Materials and Structures, 2022. 31(5): p. 055021.

15.Luo, H.C., X. Ren, Y. Zhang, X.Y. Zhang, X.G. Zhang, C. Luo, X. Cheng, and Y.M. Xie, Mechanical properties of foam-filled hexagonal and re-entrant honeycombs under uniaxial compression. Composite Structures, 2022. 280: p. 114922. https://doi.org/10.1016/j.compstruct.2021.114922.

16. Habib, F., P. Iovenitti, S. Masood, and M. Nikzad, Cell geometry effect on in-plane energy absorption of periodic honeycomb structures. The International Journal of Advanced Manufacturing Technology, 2018. 94(5): p. 2369-2380.

17. Saufi, S., M. Zuhri, M.L. Dezaki, S. Sapuan, R. Ilyas, A. As' arry, M. Ariffin, and M. Bodaghi, Compression Behaviour of Bio-Inspired Honeycomb Reinforced Starfish Shape Structures Using 3D Printing Technology. Polymers, 2021. 13(24): p. 4388.

18. Tabacu, S. and C. Ducu, Numerical investigations of 3D printed structures under compressive loads using damage and fracture criterion: Experiments, parameter identification, and validation. Extreme Mechanics Letters, 2020. 39: p. 100775.

19. Ghongade, G., K.P. Kalyan, R.V. Vignesh, and M. Govindaraju, Design, fabrication, and analysis of cost effective steel honeycomb structures.

Materials Today: Proceedings, 2021. 46: p. 4520-4526.

20. Xia, H., Q. Sun, and S. Wang, Influence of strain rate effect on energy absorption characteristics of bio-inspired honeycomb column thin-walled structure under impact loading. Case Studies in Construction Materials, 2023. 18: p. e01761. https://doi.org/10.1016/j.cscm.2022.e01761.

21. Xu, H.H., H.C. Luo, X.G. Zhang, W. Jiang, X.C. Teng, W.Q. Chen, J. Yang, Y.M. Xie, and X. Ren, Mechanical properties of aluminum foam filled re-entrant honeycomb with uniform and gradient designs. International Journal of Mechanical Sciences, 2023. 244: p. 108075. https://doi.org/10.1016/j.ijmecsci.2022.108075.

22. Ganesh, B., B. Kumar, and D. Muppala, Design and structural analysis of aircraft floor panel. International Journal of Advanced Engineering and Global Technology, 2015. 3(12): p. 1451-1460.

23. Caycedo Garcia, M.S., G.H. Siqueira, L.C.M. Vieira Junior, and I. Vizotto, Evaluation of structural capacity of triangular and hexagonal reinforced concrete free-form shells. Engineering Structures, 2019. 188: p. 519-537. https://doi.org/10.1016/j.engstruct.2019.03.044.

24. Saada, K., S. Amroune, M. Zaoui, A. Houari, K. Madani, and A. Hachaichi, Experimental and Numerical Study of the Effect of the Presence of a Geometric Discontinuity of Variable Shape on the Tensile Strength of an Epoxy Polymer. Acta Mechanica et Automatica, 2023. 17(2): p. 192-199.

25. Dong, Z., Y. Li, T. Zhao, W. Wu, D. Xiao, and J. Liang, Experimental and numerical studies on the compressive mechanical properties of the metallic auxetic reentrant honeycomb. Materials & Design, 2019. 182: p. 108036. https://doi.org/10.1016/j.matdes.2019.108036.

26. Keskin, İ., M. Yadgar Ahmed, N. Ramadhan Taher, M. Gör, and B. Zrar Abdulsamad, An evaluation on effects of surface explosion on underground tunnel; availability of ABAQUS Finite element method. Tunnelling and Underground Space Technology, 2022. 120: p. 104306. https://doi.org/10.1016/j.tust.2021.104306.

27. Siedel, D., T. Helfer, O. Fandeur, J. Besson, S. Forest, and N. Pignet. Schéma de résolution locale pour la méthode Hybrid High Order et application en mécanique non-linéaire. in 15ème colloque national en calcul des structures. 2022.

28. Hosseinabadi, H.G., R. Bagheri, L.A. Gray, V. Altstädt, and K. Drechsler, Plasticity in polymeric honeycombs made by photo-polymerization and nozzle based 3D-printing. Polymer Testing, 2017. 63: p. 163-167.

29. Colatosti, M., N. Fantuzzi, P. Trovalusci, and R. Masiani, New insights on homogenization for hexagonal-shaped composites as Cosserat continua. Meccanica, 2022. 57(4): p. 885-904. 10.1007/s11012-021-01355-x.

30. Vincent, V.A., C. Kailasanathan, V.K. Shanmuganathan, J.V.S.P. Kumar, and V.R. Arun *Prakash, Strength characterization of caryota urens fibre and aluminium 2024-T3 foil multi-stacking sequenced SiC-toughened epoxy structural composite. Biomass Conversion and Biorefinery, 2022. 12(9): p. 4009-4019. 10.1007/s13399-020-00831-w.*